Digital Object Identifier (DOI): (to be appear)

Proceedings of the IEEE Energy Conversion Congress and Exposition (ECCE 2013), Denver, CO, USA, 14-19 September, 2013.

Low Voltage Ride-Through of Single-Phase Transformerless Photovoltaic Inverters

Yongheng Yang
Frede Blaabjerg
Huai Wang

Suggested Citation

Y. Yang, F. Blaabjerg, and H. Wang "Low voltage ride-through of single-phase transformerless photovoltaic inverters," *in Proc. IEEE Energy Convers. Congr. and Expo.*, 2013, pp. 4762-4769.

Low Voltage Ride-Through of Single-Phase Transformerless Photovoltaic Inverters

Yongheng Yang, *IEEE Student Member*, Frede Blaabjerg, *IEEE Fellow*, Huai Wang, *IEEE Member*
Department of Energy Technology
Aalborg University
Pontoppidanstraede 101, Aalborg, DK-9220 Denmark
yoy@et.aau.dk, fbl@et.aau.dk, hwa@et.aau.dk

***Abstract*—Transformerless photovoltaic (PV) inverters are going to be more widely adopted in order to achieve high efficiency, as the penetration level of PV systems is continuously booming. However, problems may arise in highly PV-integrated distribution systems. For example, a sudden stoppage of all PV systems due to anti-islanding protection may trigger grid disturbances. Thus, standards featuring with ancillary services for the next generation PV systems are under a revision in some countries. The future PV systems have to provide a full range of services as what the conventional power plants do, e.g. Low Voltage Ride-Through (LVRT) under grid faults and grid support service. In order to map future challenges, the LVRT capability of three mainstream single-phase transformerless PV inverters under grid faults are explored in this paper. Control strategies with reactive power injections are also discussed. The selected inverters are the full-bridge inverter with bipolar modulation, full-bridge inverter with DC bypass and the Highly Efficient and Reliable Inverter Concept (HERIC). A 1 kW single-phase grid-connected PV system is analyzed to verify the discussions. The tests confirmed that, although the HERIC inverter is the best candidate in terms of efficiency, it is not very feasible in case of a voltage sag. The other topologies are capable of providing reactive current during LVRT. A benchmarking of those inverters is also provided, which offers the possibility to select appropriate devices and to further optimize the system.**

I. INTRODUCTION

The year of 2012 has been another year for an extraordinary growth of photovoltaic (PV) systems with total global operating capacity reaching the 100 GW milestone [1]. However, this high penetration level of PV systems may also introduce negative impacts on the grid. Concerns like power quality issues, the efficiency and the emerging reliability are becoming of high interest and intense importance [2]-[9]. Thus, many grid codes have been released to regulate PV systems integration with the distributed grid [10]-[18]. Since PV systems are typically connected to low-voltage and/or medium-voltage distributed networks, the grid standards are mainly focused on power quality issues, frequency stability and voltage stability [11]. It is required that PV systems should cease to energize local loads in presence of a grid fault, e.g. a voltage sag and a frequency disturbance [11], [15], which is known as an anti-islanding protection.

Due to the still declined PV cell price and the advanced power electronics technology, the penetration level is going to be much higher. In view of this, the impact of highly penetrated PV systems, even serving low-voltage networks, on the grid cannot be neglected anymore. A sudden stoppage of all grid-connected PV systems in an unintentional islanding operation mode could trigger much more severe grid problems than the initial event, e.g. power outages and voltage flickers [2]. In order to solve the potential issues, several European countries have updated the grid codes for low- or medium-voltage systems. The next generation PV systems have to provide a full range of services as what the conventional power plants do. For instance, the German grid code requires that the generation systems connected to the medium- or high-voltage networks should have Low Voltage Ride-Through (LVRT) capability under grid faults [15]. In the new Italian grid code, the generation units connected to low-voltage grid with the nominal power exceeding 6 kW have to ride through grid voltage faults [16]. Other countries like Japan [17]-[19] are undertaking a revision of their current active grid standards in order to accept more PV energy in the line. However, some standard committees, e.g. IEEE Standard Committee, still have some catching up to do [20].

Besides the ancillary services, achieving high efficiency and high reliability are always required in PV systems in order to reduce energy losses and extend service time [3], [7], [8], [21]. Compared to conventional PV systems, transformerless systems are increasing in popularity, especially in European markets, because of the high efficiency [11], [22]-[30]. Many transformerless topologies are derived by adding extra power devices into the Full-Bridge (FB) inverter. For example, the FB inverter with DC bypass (FB-DCBP) adds two power devices at the DC-side [23]; while the Highly Efficient and Reliable Inverter Concept (HERIC) provides an AC bypass leg [25]. Considering the fast growth of grid-connected PV systems, it is better for the next generation transformerless PV inverters to equip with LVRT capability in order to fulfill the upcoming requirements efficiently and reliably.

Current stresses, power losses on the switching devices and dynamic responses of transformer-less inverters are dependent on the topology configuration in both normal operation and LVRT operation mode. Thus, it is necessary to explore the performance of these PV systems under different conditions. In this paper, three transformerless PV inverters – FB inverter with bipolar modulation (FB-Bipolar), FB-DCBP inverter and the HERIC inverter are studied in terms of current stresses, efficiency, and LVRT capability with reactive power injection. Firstly, a brief introduction of the

selected inverters is given. Then, the focus is shifted to the control of transformerless PV systems under grid faults. Control strategies and reactive power injection possibilities for single-phase PV systems are discussed in § III. Simulation results of LVRT operation examples are demonstrated in §IV, as well as experimental tests of a FB inverter system. A benchmarking of the selected inverters in terms of leakage current elimination, LVRT capability and efficiency is presented before the conclusions.

II. Single-Phase Transformerless PV Inverters

Underpinned by the advanced and dedicated control methods, the PV inverters are responsible for converting DC source generated from PV panels to AC source efficiently and reliably. A widely adopted single-phase PV inverter is the FB topology as shown in Fig. 1, where it is connected to the grid through an *LCL*-filter in order to ensure the injected current quality. There are two main modulation strategies available for this inverter: a) unipolar modulation scheme and b) bipolar modulation scheme.

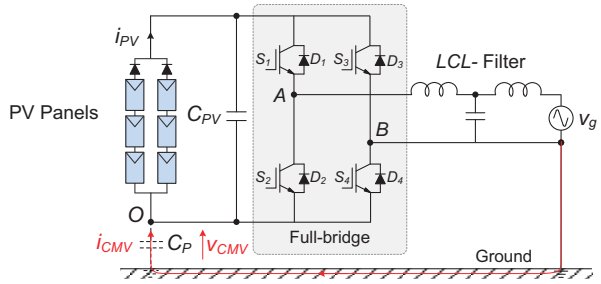

Fig. 1. A single-phase Full-Bridge (FB) grid-connected PV system with an *LCL*-filter.

When the transformer is removed from a grid-connected PV system, safety concerns (e.g. leakage current) will arise since the lack of galvanic isolations. Thus, transformerless inverters should eliminate or at least reduce the leakage current, e.g. by including passive damping components and/ or by modifying the modulations [23]. In the light of this, the FB-Bipolar is more feasible in single-phase transformerless PV applications. However, in every switching period, there are reactive power exchange between the *LCL*-filter and the capacitor C_{PV} and also core losses in the output *LCL*-filter, leading to a low efficiency of up to 96.5% [11].

In order to further improve the efficiency and reduce the leakage current, a tremendous number of transformerless topologies have been developed [11], [22]-[30], most of which are based on the FB inverter as it is shown in Fig. 1. The first priority of a transformerless inverter is to avoid the generation of a varying instantaneous Common-Mode Voltage (CMV, v_{CMV}), since the CMV will induce a common-mode current (leakage current). The relationships can simply be described as,

$$v_{CMV} = \frac{v_{AO} + v_{BO}}{2}, \tag{1}$$

$$i_{CMV} = C_P \frac{dv_{CMV}}{dt}, \tag{2}$$

where v_{AO} and v_{BO} are the voltages of the two midpoints of a FB inverter shown in Fig. 1, i_{CMV} is the common-mode current, and C_P is the stray capacitor between PV panels and the ground.

Besides those solutions to limit the leakage current by adding passive damping components and by modifying the modulation techniques, the elimination can also be achieved either by disconnecting the PV panels from the inverter or by providing a bypass leg at the AC side. For instance, the FB-DCBP inverter patented by Ingeteam [23] shown in Fig. 2(a) disconnects the PV panels from the inverter using four extra devices (two switching devices SD_5, SD_6 and two diodes D_7, D_8); while the HERIC inverter (Fig. 2(b)) by Sunways [25] provides an AC bypass using two extra switching devices (SD_5, SD_6). There have been other transformerless topologies reported in the literature. Some are based on the multi-level topologies [26]-[28], and some are derived by optimizing traditional transformerless inverters [29], [30].

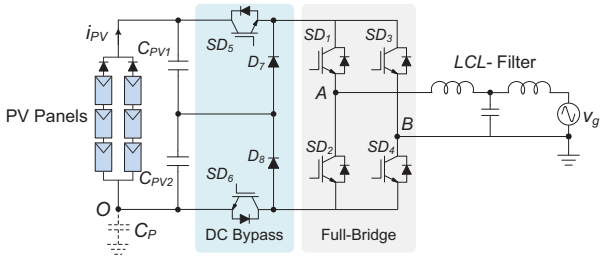

(a) Full-bridge with DC bypass topology [23]

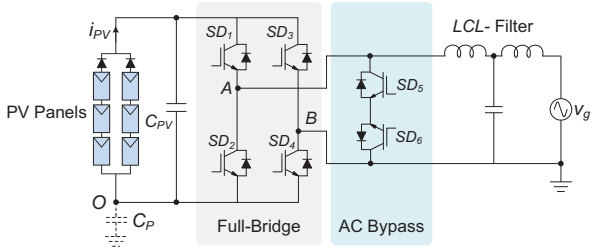

(b) Highly efficient and reliable inverter concept, HERIC [25]

Fig. 2. Two main grid-connected transformerless PV systems with *LCL*-filter (*SD*-IGBT module, *S*-IGBT, *D*-Diode).

In respect to the modulation of a transformerless inverter, it should not generate a varying CMV. With a dedicated modulation scheme for those inverters, there is no reactive power exchange between the *LCL*-filter and the capacitor C_{PV} at zero-voltage states, and thus higher efficiency is achieved. However, extra power losses, including switching losses and conduction losses, will appear on the required additional switching devices in these inverters as shown in Fig. 2. Moreover, the power losses of an individual switching device are dependent on its commutation frequency, which differs with inverter topologies, and its electrical stress. For example, the extra devices, S_5 and S_6 in the FB-DCBP inverter are commutated at a high switching frequency (e.g., 10 kHz); while those in the HERIC inverter commutate at the line fundamental frequency (e.g., 50 Hz). Since the total power losses will further introduce redistributions of both current and thermal stresses on the devices among these inverters, the efficiency and the lifetime will be affected.

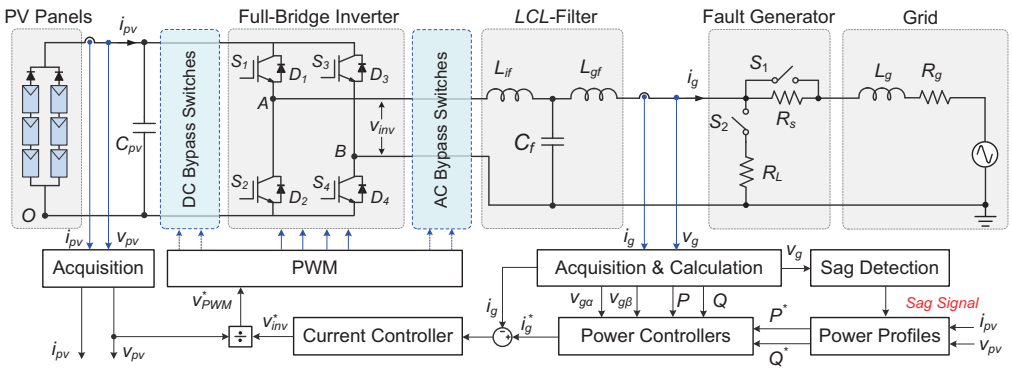

Fig. 3. Hardware schematic and control diagram of single-phase transformerless grid-connected PV systems with low voltage ride-through capability.

Concerning LVRT operation, the control systems and the dynamic response of the above inverters possibly differ with the configurations and the modulation schemes. They may have a significant impact on the capability of reactive power injection to support the grid voltage recovery under grid faults. Moreover, the overstresses on the switching devices may also cause failures during LVRT and thus increase the maintenance cost. Those aspects should be taken into consideration for the design and operation of transformerless PV systems. Thus, essentially, this paper explores the performance of the mainstream transformerless inverters with the consideration of such operation conditions.

III. Control of Transformerless PV Inverters under Grid Faults

According to the grid requirements, the design of next generation transformerless PV systems should take into account not only the shape of grid current (power quality issues), but also the behavior of reactive power injection under grid faults. Fig. 3 shows the hardware schematic and overall control structure of a single-phase transformerless PV system with LVRT capability.

Typically, the control strategy applied to a single-phase grid-connected system includes two cascaded loops [11], [12]:

a) An inner current control loop, which has the responsibilities of power quality issues and current protection of the inverter and,
b) An outer voltage control (or power control) loop, in which the grid voltage is controlled to generate desired current references for the inner control loop.

A. Current Control Loop

For the current control loop, the existing control methods, such as Proportional Resonant (PR), Resonant Control (RSC), Repetitive Controller (RC), and Deadbeat Controller (DB) can be adopted directly [12], [15], [31]. Further, applying the Park transformation lead to the possibility of Proportional Integral (PI) controllers to regulate the injected current, and afterwards, the modulation reference v^*_{inv} can be obtained by means of the inverse Park transformation. Since the current control loop is responsible for the power quality, this responsibility should also be effective and valid in the design of current controllers and also the *LCL*-filter. By introducing harmonic compensators for the controller and adding passive damping for the filter, an enhancement of the current controller tracking performance can be achieved.

Since the PR controller with Harmonic Compensators (PR+HC) presents a good performance in terms of accurate tracking and fast dynamic response [11], [12], this controller is selected in this paper as the inner current controller. The transfer function of this controller can be given as,

$$G_i(s) = k_p + k_r \frac{s}{s^2+\omega_0^2} + \sum_{h=3,5,7} \frac{k_{rh} s}{s^2+(h\omega_0)^2}, \quad (3)$$

in which k_p is the proportional gain, k_r is the fundamental resonant control gain, k_{rh} is the control gain for h-order resonant controller ($h = 3, 5, 7$) and ω_0 is the grid fundamental frequency.

B. Voltage Control Loop (Power Control Loop)

For the outer voltage control loop, it provides the system operation conditions (e.g. grid voltage amplitude and grid frequency) and then it generates a current reference, which is subsequently utilized in the inner current control loop. Thus, it offers the possibilities to add control methods into this loop to shape the grid current in LVRT operation mode with the purpose of reactive power injection. For example, based on the single-phase *PQ* theory [9], [15], the injected grid current reference can be produced by regulating the averaged active power and reactive power, as it is shown in Fig. 3. This power control method is intuitive and simple, since the averaged active power and the averaged reactive power references (P^* and Q^*) can directly be set by the operators. With the help of orthogonal signal generator systems (e.g. Hilbert transform) [9], [11], the grid current reference i^*_g can be expressed as,

$$i^*_g = \frac{1}{v_{g\alpha}^2 + v_{g\beta}^2} \begin{bmatrix} v_{g\alpha} & v_{g\beta} \end{bmatrix} \begin{bmatrix} G_P(s)(P-P^*) \\ G_Q(s)(Q-Q^*) \end{bmatrix}, \quad (4)$$

where $v_{g\alpha}$, $v_{g\beta}$ are the orthogonal components of the grid voltage, respectively, P, Q are the averaged active power and reactive power, P^*, Q^* are the power references and $G_P(s)$, $G_Q(s)$ are PI-based controllers for the active power and the reactive power, respectively.

There are also other control possibilities available for the outer control loop of a single-phase system, such as the droop-based control and the instantaneous power control [32]-[35]. The droop-based power control method is implemented based on the assumption that the distributed line is mainly inductive [32]. However, in fact, the PV systems have been dominated by residential applications with low rated power and low voltage grid. In the case of those applications, such assumption is not valid. The instantaneous power control method acts directly on the instantaneous power, and subsequently the reference current is produced. Thus, there is no need to calculate the averaged active power and reactive power for this method [34]. It may be a good candidate for single-phase applications in LVRT operation mode.

Nevertheless, in regard to the above control methods, e.g. the *PQ* control strategies, a fast voltage sag detection and an accurate synchronization system will strongly contribute to the dynamic performance and the stability margin of the whole control systems. Even for the instantaneous power control method, the syntheses of instantaneous power reference from the averaged active power and reactive power references is affected by the knowledge of grid conditions.

C. Reactive Power Injection Strategies

The "*Power Profiles*" unit in Fig. 3 is used to generate the average active power and reactive power references for the power controllers, and subsequently, the references are controlled to produce the grid current reference as discussed previously. In the normal operation mode, the average active power reference P^* is the output of a Maximum Power Point Tracking (MPPT) system and the whole system is required to operate at unity power factor.

When a grid voltage fault is detected by the "*Sag Detection*" unit, the PV system enters into the LVRT operation mode. It is required by the grid codes that the system should withstand the voltage drop for a specified short period, as it is shown in Fig. 4. At the same time, the PV system should inject reactive power (current) to support the grid voltage recovery [9], [15]-[19]. Fig. 5 shows an example of the required reactive power injection during LVRT for medium- and high-voltage wind turbine power systems specified in the German E.ON grid code. According to the requirements defined in Fig. 5, the averaged reactive power reference Q^* is a function of the grid voltage level in LVRT operation mode. Then it is controlled and injected into the grid to support the voltage recovery.

For three-phase applications, the reactive power injection strategies can be summarized as: 1) unity power factor control strategy, 2) positive and negative sequence control strategy, 3) constant active power control strategy and 4) constant reactive power control strategy [11], [12], [36]-[39]. Unbalanced grid conditions are opt to occur in three-phase systems. Since there is an interaction between voltage sequences and current sequences under grid faults, either the controlled active power or the controlled reactive power will present oscillations [41]. Thus, in [41], the zero-sequence control path has been introduced to further increase the control freedoms and to eliminate the oscillations in the controlled power.

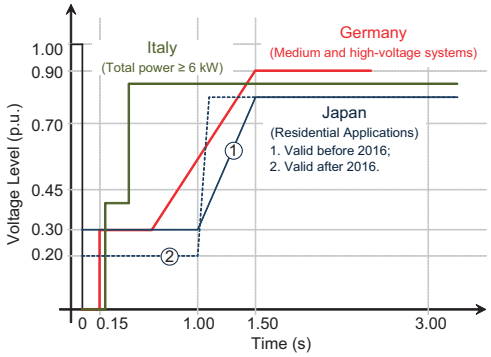

Fig. 4. Low voltage ride-through requirements defined in different countries covering a wide range of applications [9], [15].

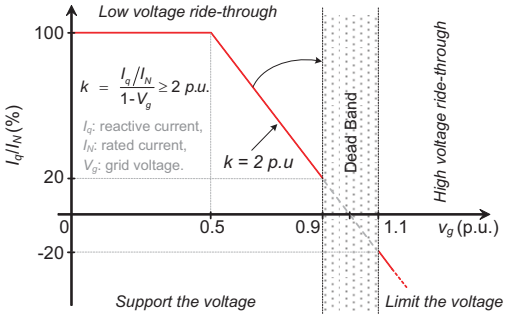

Fig. 5. Reactive current injection requirements for medium- and/or high-voltage wind turbine power systems defined in E.ON grid code [10].

For single-phase systems, there are even less control freedoms (grid voltage and grid current). By considering the over-current protection of PV inverters and the reactive current injection requirements under grid faults, possibilities for reactive power injection of single-phase PV systems are:

1) Constant Peak Current Strategy

With this control strategy, there is no risk of inverter shutdown due to overcurrent protection, since the peak of the injected grid current (I_{gmax}) is kept constant during LVRT. The injected reactive current level (I_q) is calculated according to Fig. 5. The grid peak current I_{gmax} can be set as the rated current level I_N of the PV system, for example,

$$\begin{cases} I_{g\max} = I_N \\ I_q = k\left(1-v_g\right)I_N \end{cases}, \tag{5}$$

in which v_g is the grid voltage, 0.5 p.u. $\leq v_g \leq$ 0.9 p.u., and $k \geq 2$ p.u.. According to Fig. 5, the PV inverter should generate full reactive power (I_q=I_N) when v_g < 0.5 p.u.. The phasor diagram for this control strategy is shown in Fig. 6(b), from which it can be observed that the output active power decreases (I_d<I_N and V_g<V_{gn}) during LVRT.

2) Constant Active Current Strategy

Another control possibility under LVRT operation is to keep the active current constant. For the purpose to extract as much energy from the PV panels as possible, for example, the level of active current can be controlled to be that of the rated current (I_d=I_N), as it is shown in Fig. 6(c). The injected

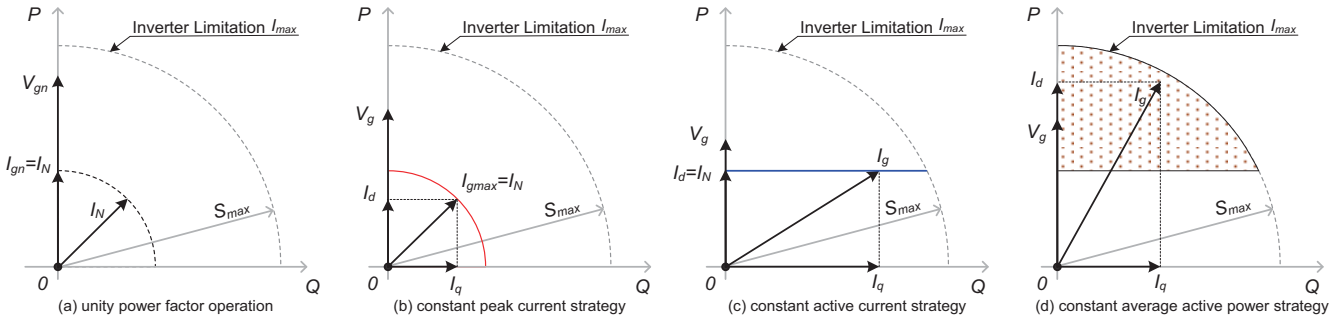

Fig. 6. Representations of the grid current and the grid voltage of a single-phase PV system with different reactive power injection strategies ($v_g \geq 0.5$ p.u.).

reactive current (I_q) is proportional to the voltage sag depth in a certain voltage range (0.5 p.u. $\leq v_g \leq$ 0.9 p.u.), as it is shown in Fig. 5. With this reactive power injection strategy, the amplitude of the injected current may exceed the inverter limitation (I_{max}). In order to avoid inverter shutdown due to over-current protection, the following should be fulfilled during the design and the operation of a PV inverter,

$$\sqrt{1+k^2\left(1-v_g\right)^2} \leq \frac{I_{\max}}{I_N}, \tag{6}$$

where v_g is the grid voltage and $k \geq 2$ p.u..

Considering a pre-designed inverter with a robustness margin, $I_{max} = 1.5I_N$, and $k = 2$ p.u., it is not possible to utilize this control strategy to inject the required reactive power, since the minimum margin is 2.06 for $k = 2$ p.u.. In such a case, the PV system should also de-rate the active power output in order to generate enough reactive power. Otherwise, over-rated operations may introduce failures to the whole system and shorten the inverter serving time, and thus the maintenance cost increases.

3) *Constant Average Active Power Strategy*

Similar to the constant active current control strategy, a more intuitive way to maximize output energy (i.e., to deliver maximum active power) is to keep the average active power constant during LVRT. However, the required injection of reactive power might pose a risk of over-current protection with this control strategy. Under this situation, the currents can be expressed as,

$$\begin{cases} I_d = \dfrac{1}{v_g} I_N \\ I_q = k\left(1-v_g\right) I_N \end{cases}, \tag{7}$$

in which v_g and k are defined previously. Thus, the following constraint should be satisfied to avoid inverter shutdown due to over-current protection.

$$\frac{1}{v_g}\sqrt{1+k^2\left(v_g-v_g^2\right)^2} \leq \frac{I_{\max}}{I_N}. \tag{8}$$

During the design and the operation of the PV inverters, those above constraints should be considered. Especially, for the next generation PV systems, the provision of reactive power both in normal operation and under grid faults, and the requirements of LVRT will come into force in the near future. If those above aspects are not well considered, the maintenance costs and energy losses may increase.

IV. Simulation and Experimental Results

Fig. 7 presents the closed loop control system for a single-phase transformerless PV system. It is observed in Fig. 7 that an effective power calculation method in terms of fast dynamic response and accurate computation, together with an advanced synchronization unit, can contribute to the LVRT performance of the entire system. In this paper, the Second Order Generalized Integrator based Phase Locked Loop (SOGI-PLL) has been selected as the synchronization unit because of its robustness [9], [11], [12]. The average power calculations are based on the Discrete Fourier Transformation (DFT). Since the DFT uses a running window to do the calculation, it naturally will introduce a delay [41]. The other parameters are listed in TABLE I. A voltage fault (0.43 p.u.) is generated by switching S_1 and S_2 of the sag generator shown in Fig. 3.

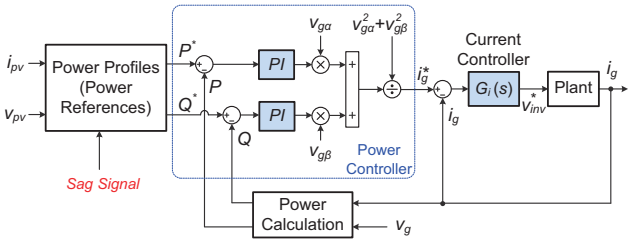

Fig. 7. Closed loop control system of a single-phase transformerless system with low voltage ride through capability based on the single-phase *PQ* theory and PR+HC current controller.

The control system has been implemented in a dSPACE DS 1103 system. A Danfoss three-phase VLT FC300 inverter is used in the experiments as the power conversion stage. A Delta DC source is adopted, and the DC voltage is 400 V. Simulations are firstly tested in MATLAB/Simulink using PLECS blockset for the modelling. During LVRT operation, the control system sets the reference power according to a detected voltage sag depth, and the system will start to inject reactive power into the grid once the fault is confirmed. In the cases, the voltage sag is 0.43 p.u., and thus according to Fig. 5 and Fig. 6, the average reactive power Q^* should be 490.2 Var during LVRT, and the active power P^* should be 290 W when the constant peak current control strategy is adopted. The simulation results are shown in Fig. 8 and Fig. 9.

TABLE I. SIMULATION AND EXPERIMENTAL PARAMETERS.

Normal Grid Voltage	$V_g = 230\ V$
Normal Grid Frequency	$\omega_0 = 2\pi \times 50\ rad/s$
Grid Impedance	$L_g = 2\ mH$, $R_g = 0.04\ \Omega$
Rated Power	$P_n = 1\ kW$
Switching Frequency	$f_{sw} = 10\ kHz$
LCL-Filter	$L_{if} = 3.6\ mH$, $L_{gf} = 708\ \mu H$, $C_f = 2.35\ \mu F$
Sag Generator	$R_S = 19.3\ \Omega$, $R_L = 19.9\ \Omega$
PI based Power Controllers	$k_{pp} = 1.5$, $k_{ip} = 52$ of $G_P(s)$ - active power $k_{pq} = 1$, $k_{iq} = 50$ of $G_Q(s)$ - reactive power
PR+HC Current Controller	$k_p = 20$, $k_r = 2000$, $k_{r3,5,7} = 5000$

As it is shown in Fig. 8 and Fig. 9, in a wide range of grid voltage level, the FB-Bipolar inverter can provide required reactive power during LVRT operation. The FB-DCBP inverter is also capable of riding through the voltage sag within a voltage range of 0.5 p.u. to 0.9 p.u.. However, it also presents a varying v_{CMV} (high leakage current) under grid fault as shown in Fig. 9(b). Moreover, the current stresses on the extra devices of FB-DCBP are significantly higher the four devices of a FB inverter, as it is shown in Fig. 8. The high stresses might induce failures to the whole inverter. Since the HERIC inverter is disconnected from the grid when the transformerless inverter is also short-circuited in order to avoid leakage currents, the inverter cannot provide reactive power in LVRT operation. This is also verified in Fig. 9(c), in which the grid current is severely distorted at voltage zero-crossing points. Therefore, in view of this, the HERIC transformerless inverter is not special suitable for use in single-phase systems in LVRT operation with reactive power injection. However, it can achieve a high efficiency among these three topologies operating at unity power factor, which

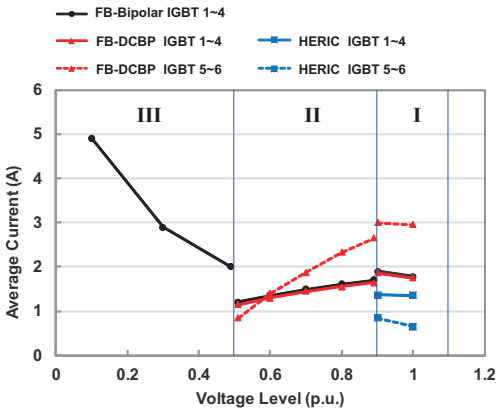

Fig. 8. Average current stresses of IGBT devices in the three transformerless PV with different voltage levels: I- normal operation (0.9 p.u.$\leq v_g <$ 1.1 p.u.), II-LVRT with constant peak current control (0.5 p.u.$\leq v_g <$ 0.9 p.u.), and III-full reactive power injection ($v_g <$ 0.5 p.u.).

can be observed from Fig. 8 where the current stress is shown and the benchmarking results in TABLE II. Due to the lowest current stresses on the FB devices and the extra devices, a cost-effective design can be achieved for HERIC inverter in the normal operation.

Fig. 10 and Fig. 11 show the experimental results for a single-phase FB system. It can be seen from Fig. 10 that by applying bipolar modulation strategy, the CMV of a FB inverter has been kept constant. Thus, it would not generate leakage currents. Fig. 11 demonstrates that the FB inverter is capable of riding through a low-voltage fault. It can inject the required reactive power into the grid and at the same time the average active power generation is limited. Since the constant peak current control strategy is used in the tests, the amplitude

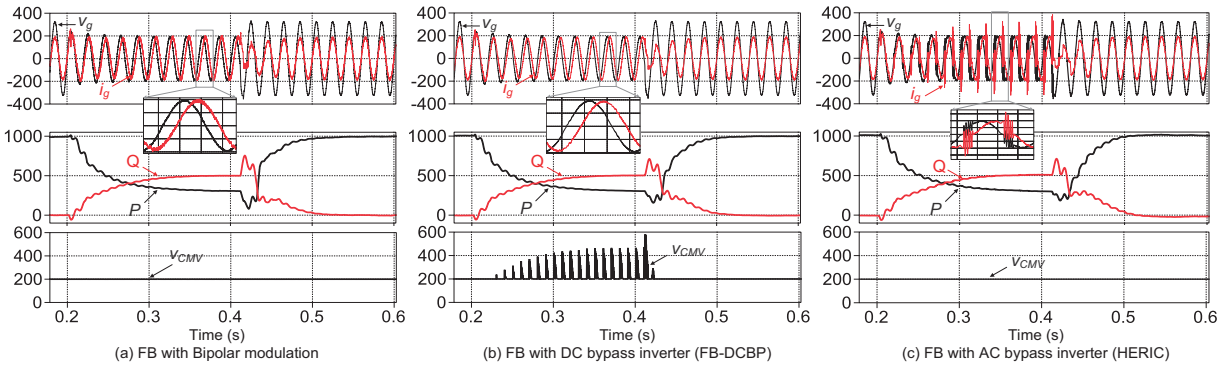

Fig. 9. Performance of the three grid-connected transformerless PV systems in low voltage ride through operation (0.43 p.u. voltage sag): grid voltage v_g [V], grid current i_g [30×A], active power P [W], reactive power Q [Var], and common mode voltage v_{CMV} [V].

TABLE II. BENCHMARKING OF THE THREE TRANSFORMERLESS INVERTERS.

	FB-Bipolar	FB-DCBP	HERIC
Efficiency*	97.61 %	97.67%	98.29%
LVRT Capability (Reactive power injection)	YES (full range)	YES (only when grid voltage level > 0.5 p.u.)	NO
Leakage Current (CMV)	Low (CMV = *const.*)	Low (in normal operation, CMV = *const.*) High (in LVRT, CMV ≠ *const.*)	Low (CMV = *const.*)
Device Current Stresses	-	$S_{1\sim4}$: High, $S_{5,6}$: Very High	$S_{1\sim4}$: Low, $S_{5,6}$: Low
Device Switching Freq. (f_s)	$S_{1\sim4}$: High f_s	$S_{1\sim4}$: Line Freq., $S_{5,6}$: High f_s	$S_{1\sim4}$: High f_s, $S_{5,6}$: Line Freq.

* Conversion efficiency by only considering the losses on the power devices. Rated power: 1 kW, DC voltage: 400 V.

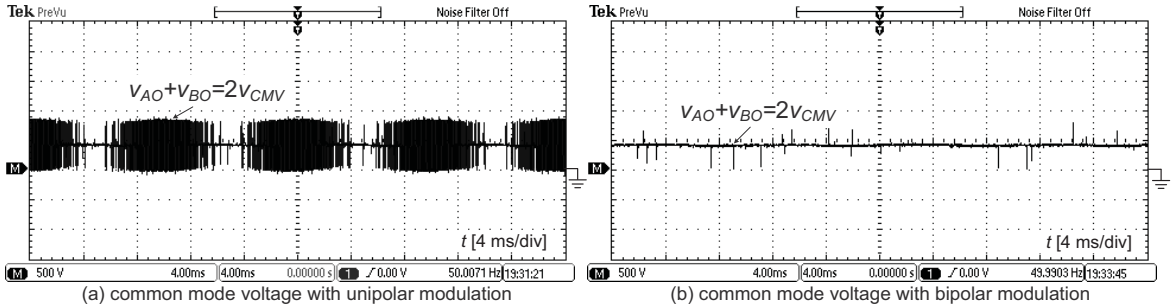

(a) common mode voltage with unipolar modulation (b) common mode voltage with bipolar modulation

Fig. 10. Common mode voltage of a 1 kW full-bridge inverter (DC voltage: 400 V) with different modulation strategies: v_{CMV} [500 V/div]

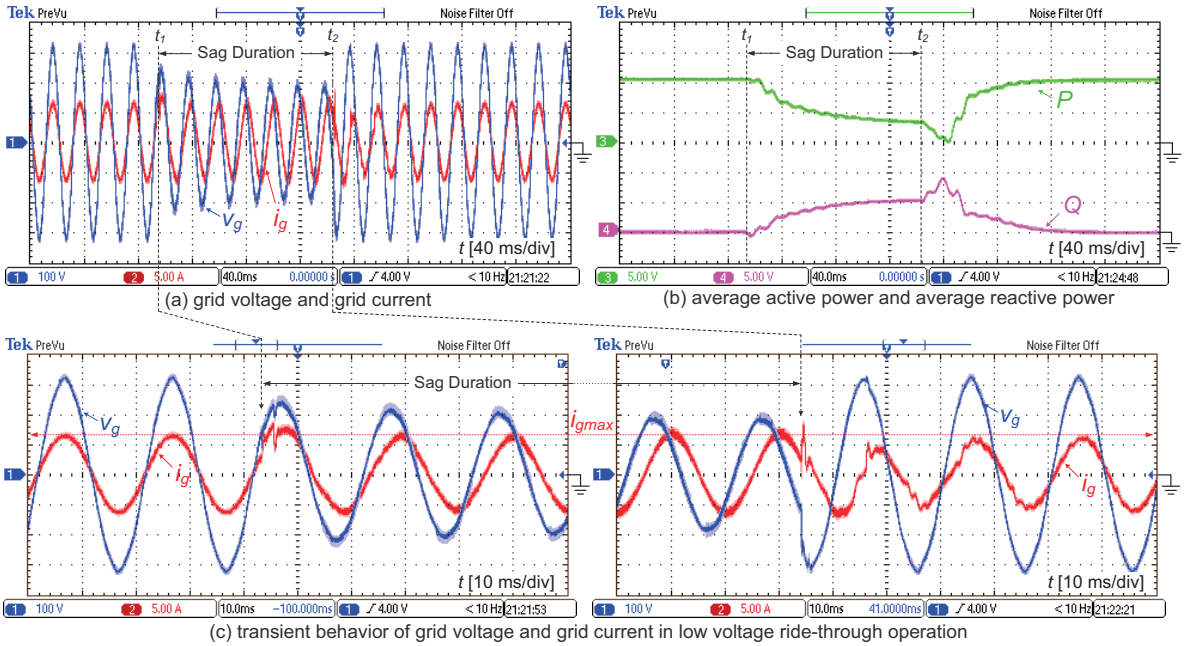

Fig. 11. Low voltage ride through operation of a 1 kW single-phase full-bridge system with bipolar modulation and constant peak current control strategy (0.43 p.u. voltage sag): (a) grid voltage v_g [100 V/div] and grid current i_g [5 A/div], (b) average active power P [500 W/div] and average reactive power Q [500 Var/div], and (c) transient behavior of grid voltage v_g [100 V/div] and grid current i_g [5 A/div].

of the grid current is kept constant during LVRT, which validates its effectiveness. When the voltage sag is cleared, the power control method based on the single-phase PQ theory can fast change the system to unity power factor operation. However, due to the power calculation delay and the frequency swing, the transient current presents severe distortions, especially during voltage recovery. Nevertheless, those tests demonstrate the effectiveness of the power control method and the reactive power injection strategy used in this paper in terms of fast response and feasible compliance to the grid requirements.

V. Conclusions

The Low Voltage Ride-Through (LVRT) capability of three mainstream single-phase transformerless PV inverters has been explored in this paper. A benchmarking of those inverters has also been presented in terms of efficiency, LVRT capability, current stresses and leakage current rejection.

With respect to the reactive power injection control, three possibilities have been discussed. The constant peak current control strategy has been verified by experiments. The results show that the HERIC inverter can achieve a high efficiency, but it cannot be used in the next generation PV systems with LVRT capability or reactive power injection. For this inverter, a possible way to ride-through voltage fault is to modify the modulation scheme during LVRT but at the cost of reducing efficiency. The performance of a Full-Bridge inverter with DC bypass topology (FB-DCBP) is satisfactory under LVRT operation. It can achieve a slightly higher efficiency compared to full-bridge inverter with bipolar modulation. However, in LVRT operation, a varying common mode voltage appears in the FB-DCBP inverter, which may introduce safety problems. Moreover, due to the high switching frequency for the extra devices of the FB-DCBP, high current stresses might appear and further introduce failures to the whole system.

Nevertheless, for different applications, the presented benchmarking result provides a convenient way to select appropriate devices of those inverters. The test results have verified the effectiveness of the PQ control method and the constant peak current strategy for reactive power injection.

References

[1] REN21, "Renewables 2013: Global Status Report (GSR) ," [Online]. Available: http://www.ren21.net/, Jun. 2013.

[2] K.O. Kovanen, "Photovoltaics and power distribution," *Renewable Energy Focus*, vol. 14, no. 3, pp. 20-21, May/Jun. 2013.

[3] Y. Xue, K.C. Divya, G. Griepentrog, M. Liviu, S. Suresh, and M. Manjrekar, "Towards next generation photovoltaic inverters," in *Proc. of ECCE'11*, pp. 2467-2474, 17-22 Sept. 2011.

[4] S.-M. Chen, T.-J. Liang, and K.-R. Hu, "Design, analysis, and implementation of solar power optimizer for DC distribution system," *IEEE Trans. Power Electron.*, vol. 28, no. 4, pp. 1764-1772, Apr. 2013.

[5] P.S. Shenoy, K.A. Kim, B.B. Johnson, and P.T. Krein, "Differential power processing for increased energy production and reliability of photovoltaic systems," *IEEE Trans. Power Electron.*, vol. 28, no. 6, pp. 2968-2979, Jun. 2013.

[6] E. Koutroulis and F. Blaabjerg, "Design optimization of transformerless grid-connected PV inverters including reliability," *IEEE Trans. Power Electron.*, vol. 28, no. 1, pp. 325-335, Jan. 2013.

[7] H. Wang, M. Liserre, and F. Blaabjerg, "Toward reliable power electronics: challenges, design tools, and opportunities," *IEEE Ind. Electron. Mag.*, vol. 7, no. 2, pp. 17-26, Jun. 2013.

[8] V. Salas and E. Olías, "Overview of the state of technique for PV inverters used in low voltage grid-connected PV systems: Inverters below 10 kW," *Renewable and Sustainable Energy Reviews*, vol. 13, no. 6–7, pp. 1541-1550, Aug./Sept. 2009.

[9] Y. Yang, F. Blaabjerg, and Z. Zou, "Benchmarking of grid fault modes in single-phase grid-connected photovoltaic systems", *IEEE Trans. Ind. Appl.*, early access, Sept./Oct. 2013.

[10] T. Neumann, and I. Erlich, "Modelling and control of photovoltaic inverter systems with respect to German grid code requirements," in *Prof. of IEEE PES General Meeting*, pp. 1-8, 22-26 Jul. 2012.

[11] R. Teodorescu, M. Liserre, and P. Rodriguez, *Grid converters for photovoltaic and wind power systems*. Wiley - IEEE, 2011.

[12] F. Blaabjerg, R. Teodorescu, M. Liserre, and A.V. Timbus, "Overview of control and grid synchronization for distributed power generation systems," *IEEE Trans. Ind. Electron.*, vol. 53, no. 5, pp. 1398-1409, Oct. 2006.

[13] J. Eloy-Garcia Carrasco, J.M. Tena, D. Ugena, J. Alonso-Martinez, D. Santos-Martin, and S. Arnaltes, "Testing low voltage ride through capabilities of solar inverters," *Electric Power Systems Research*, vol. 96, pp. 111-118, Mar. 2013.

[14] E.J. Coster, J.M.A. Myrzik, B. Kruimer, and W.L. Kling, "Integration issues of distributed generation in distribution grids, " in *Proceedings of the IEEE*, vol. 99, no. 1, pp. 28-39, Jan. 2011.

[15] Y. Yang and F. Blaabjerg, "Low voltage ride-through capability of a single-stage single-phase photovoltaic system connected to the low-voltage grid," *Int'l Journal of Photoenergy*, vol. 2013, 9 papges, 2013. Open Access. Available: http://dx.doi.org/10.1155/2013/257487.

[16] Comitato Elettrotecnico Italiano, "Reference technical rules for connecting users to the active and passive LV distribution companies of electricity," [Online]. Available: http://www.ceiweb.it/, 2011.

[17] H. Kobayashi, "Fault ride through requirements and measures of distributed PV systems in Japan," in *Proc. of IEEE PES General Meeting*, pp. 1-6, 22-26 Jul. 2012.

[18] K. Fujii, N. Kanao, T. Yamada, and Y. Okuma, "Fault ride through capability for solar inverters," in *Proc. of EPE'11,* pp. 1-9, 2011.

[19] Y. Miyamoto, "Technology for high penetration residential PV systems on a distribution line in Japan," in *Proc. of the 5th Int'l Conf. on Integration of Renewable and Distributed Energy Resources,* 4-6 Dec. 2012.

[20] A. Ellis, "PV interconnection in the US: IEEE Standard 1547 Status and Outlook," in *Proc. of the 5th Int'l Conf.on Integration of Renewable and Distributed Energy Resources,* 4-6 Dec. 2012.

[21] S.B. Kjaer, J.K. Pedersen, and F. Blaabjerg, "A review of single-phase grid-connected inverters for photovoltaic modules," *IEEE Trans. Ind. Appl.,* vol. 41, no. 5, pp. 1292-1306, Sept./Oct. 2005.

[22] S.V. Araujo, P. Zacharias, and R. Mallwitz, "Highly efficient single-phase transformerless inverters for grid-connected PV systems," *IEEE Trans. Ind. Electron.*, vol. 57, no. 9, pp. 3118-3128, Sept. 2010.

[23] R. Gonzalez, J. Lopez, P. Sanchis, and L. Marroyo, "Transformerless inverter for single-phase photovoltaic systems," *IEEE Trans. Power Electron.*, vol. 22, no. 2, pp. 693-697, Mar. 2007.

[24] T. Kerekes, R. Teodorescu, P. Rodriguez, G. Vazquez, and E. Aldabas, "A new high-efficiency single-phase transformerless PV inverter topology," *IEEE Trans. Ind. Electron.*, vol. 58, no. 1, pp. 184-191, Jan. 2011.

[25] H. Schmidt, S. Christoph, and J. Ketterer, "Current inverter for direct/alternating currents, has direct and alternating connections with an intermediate power store, a bridge circuit, rectifier diodes and a inductive choke," German Patent DE10 221 592 A1, 4 Dec. 2003.

[26] I. Patrao, E. Figueres, F. Gonzalez-Espin, and G. Garcera, "Transformerless topologies for grid-connected single-phase photovoltaic inverters," *Renewable and Sustainable Energy Reviews*, vol. 15, no. 7, pp. 3423-3431, Sept. 2011.

[27] L. Zhang, K. Sun, L. Feng, H. Wu, and Y. Xing, "A family of neutral point clamped full-bridge topologies for transformerless photovoltaic grid-tied inverters," *IEEE Trans. Power Electron.*, vol. 28, no. 2, pp. 730-739, Feb. 2013.

[28] B. Gu, J. Dominic, J.-S. Lai, C.-L. Chen, T. LaBella, and B. Chen, "High reliability and efficiency single-phase transformerless inverter for grid-connected photovoltaic systems," *IEEE Trans. Power Electron.*, vol. 28, no. 5, pp. 2235-2245, May 2013.

[29] S. Saridakis, E. Koutroulis, and F. Blaabjerg, "Optimal design of modern transformerless PV inverter topologies," *IEEE Trans. Energy Conversion*, vol. 28, no. 2, pp. 394-404, Jun. 2013.

[30] B. Ji, J.Wang, and J. Zhao, "High-efficiency single-phase transformerless PV H6 inverter with hybrid modulation method," *IEEE Trans. Ind. Electron.*, vol. 60, no. 5, pp. 2104-2115, May 2013.

[31] Y. Yang, K. Zhou, and F. Blaabjerg, "Harmonics suppression for single-phase grid-connected PV systems in different operation modes," in *Proc. of APEC'13*, pp. 889-896, 17-21 Mar. 2013.

[32] R.A. Mastromauro, M. Liserre, T. Kerekes, and A. Dell'Aquila, "A single-phase voltage-controlled grid-connected photovoltaic system with power quality conditioner functionality," *IEEE Trans. Ind. Electron.*, vol. 56, no. 11, pp. 4436-4444, Nov. 2009.

[33] R. Majumder, "Reactive power compensation in single-phase operation of microgrid," *IEEE Trans. Ind. Electron.*, vol. 60, no. 4, pp. 1403-1416, Apr. 2013.

[34] S.A. Khajehoddin, M. K. Ghartemani, A. Bakhshai, and P. Jain, "A power control method with simple structure and fast dynamic response for single-phase grid-connected DG systems," *IEEE Trans. Power Electron*., vol. 28, no. 1, pp. 221-233, Jan. 2013.

[35] Y.-S. Wu, C.-H. Chang, Y.-M. Chen, C.-S. Cheng, C.-W. Liu, and Y.-R. Chang, "The current control of PV inverter for low voltage ride through," in *Proc. of EPE/PEMC*, pp. LS1d.4-1-LS1d.4-6, Sept. 2012.

[36] P. Rodriguez, A.V. Timbus, R. Teodorescu, M. Liserre, and F. Blaabjerg, "Flexible active power control of distributed power generation systems during grid faults," *IEEE Trans. Ind. Electron.*, vol. 54, no. 5, pp. 2583-2592, Oct. 2007.

[37] G.M.S. Azevedo, G. Vazquez, A. Luna, D. Aguilar, and A. Rolan, "Photovoltaic inverters with fault ride-through Capability," in *Proc. of ISIE'09*, pp. 549-553, 5-8 Jul. 2009.

[38] C.H. Benz, W.-T. Franke, and F.W. Fuchs, "Low voltage ride through capability of a 5 kW grid-tied solar inverter," in *Proc. of EPE/PEMC*, pp. T12-13-T12-20, 6-8 Sept. 2010.

[39] X. Bao, P. Tan, F. Zhuo, and X. Yue, "Low voltage ride through control strategy for high-power grid-connected photovoltaic inverter," in *Proc. of APEC'13*, pp. 97-100, 17-21 Mar. 2013.

[40] H.-C. Chen, C.-T. Lee, P.T. Cheng, R.Teodorescu, F. Blaabjerg, and S. Bhattacharya, "A flexible low-voltage ride-through operation for the distributed generation converters," in *Proc. of PEDS'13*, pp. 1354-1359, 22-25 Apr. 2013.

[41] K. Ma, M. Liserre, and F. Blaabjerg, "Power controllability of three-phase converter with unbalanced AC source," in *Proc. of APEC'13*, pp. 342-350, 17-21 Mar. 2013.

[42] Y. Yang and F. Blaabjerg, "A new power calculation method for single-phase grid-connected systems," in *Proc. of ISIE'13*, pp. 1-6, 28-31 May 2013.